ACS APPLIED MATERIALS & INTERFACES

Open Access
This article is licensed under CC-BY-NC-ND 4.0

www.acsami.org
Research Article

4D Printed Shape-Memory Elastomer for Thermally Programmable Soft Actuators

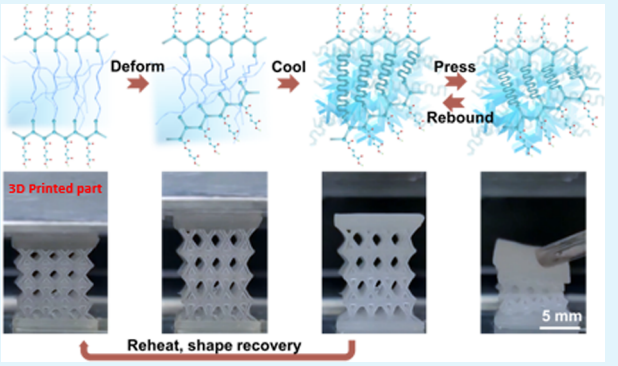
Qingchuan Song, Yunong Chen, Viacheslav Slesarenko, Pang Zhu, Ahmed Hamza, Peilong Hou, Dorothea Helmer, Frederik Kotz-Helmer,* and Bastian E. Rapp

Cite This: ACS Appl. Mater. Interfaces 2023, 15, 40923−40932

Read Online

ACCESS | Metrics & More | Article Recommendations | Supporting Information

ABSTRACT: Polymeric shape-memory elastomers can recover to a permeant shape from any programmed deformation under external stimuli. They are mostly cross-linked polymeric materials and can be shaped by three-dimensional (3D) printing. However, 3D printed shape-memory polymers so far only exhibit elasticity above their transition temperature, which results in their programmed shape being inelastic or brittle at lower temperatures. To date, 3D printed shape-memory elastomers with elasticity both below and above their transition temperature remain an elusive goal, which limits the application of shape-memory materials as elastic materials at low temperatures. In this paper, we printed, for the first time, a custom-developed shape-memory elastomer based on polyethylene glycol using digital light processing, which possesses elasticity and stretchability in a wide temperature range, below and above the transition temperature. Young's modulus in these two states can vary significantly, with a difference of up to 2 orders of magnitude. This marked difference in Young's modulus imparts excellent shape-memory properties to the material. The difference in Young's modulus at different temperatures allows for the programming of the pneumatic actuators by heating and softening specific areas. Consequently, a single actuator can exhibit distinct movement modes based on the programming process it undergoes.



KEYWORDS: *4D printing, shape memory polymers, shape memory elastomers, digital light processing, programmable pneumatic actuators*

Downloaded via UNIV FREIBURG on January 10, 2025 at 13:53:26 (UTC).
See https://pubs.acs.org/sharingguidelines for options on how to legitimately share published articles.

INTRODUCTION

Owing to their spontaneous locomotor ability actuated by specific external stimuli, shape-memory materials (SMMs) are considered as candidates for fabricating new soft robotics,[1,2] automobiles,[3] minimally invasive surgical device,[4,5] drug-release carriers,[6] smart textiles,[7] information carriers,[8] etc. Shape-memory elastomers (SMEs) are a category of polymer materials with low Young's Moduli and high stretchability.[9] 3D printing of SME has attracted significant attention due to its potential that allows the production of highly morphologically complex parts via 4D printing, i.e., printing a component with a shape that can be changed over time.[10,11] Different 3D printing technologies have been used such as fused filament fabrication (FDM),[12,13] direct ink writing (DIW),[14,15] PolyJet,[16] and vat polymerization including stereolithography (SLA) and digital light processing (DLP).[17,18] Although FDM-based 3D printing techniques are cost-effective and convenient to implement, they are, however, limited to thermoplastic materials,[19] while its contour-structuring-based slicing mode makes it difficult to reduce its structural resolution to below the millimeter level.[20] DIW, the gravity-induced structure deformation, impedes the building of truly 3D complex structures.[21] Also, the manufacturing process of DIW causes a huge gulf between its print resolution and structural resolution, e.g., with a 0.4 mm sized nozzle, resolvable print structures up to 10 mm are required.[22] Furthermore, as the accuracy of DIW increases, there is a concomitant requirement for smaller needle extrusion sizes, which inevitably leads to longer print times. Consequently, the applicability of DIW as a polymer 3D printing solution is more aligned with laboratory settings rather than the large-scale additive manufacturing production. PolyJet is usually limited to resolutions in the millimeter scale as the components often see significant distortion when printing structures smaller than 750 μm.[23] For material developers, a viable solution that strikes a balance between print accuracy and speed is the implementation of SLA or DLP techniques. These devices offer advantages such as low costs, open-source availability, and compatibility with a diverse array of resin materials, thus providing a versatile platform for experimentation and application. These two vat-based methods

Received: May 24, 2023
Accepted: July 6, 2023
Published: August 18, 2023



© 2023 The Authors. Published by American Chemical Society

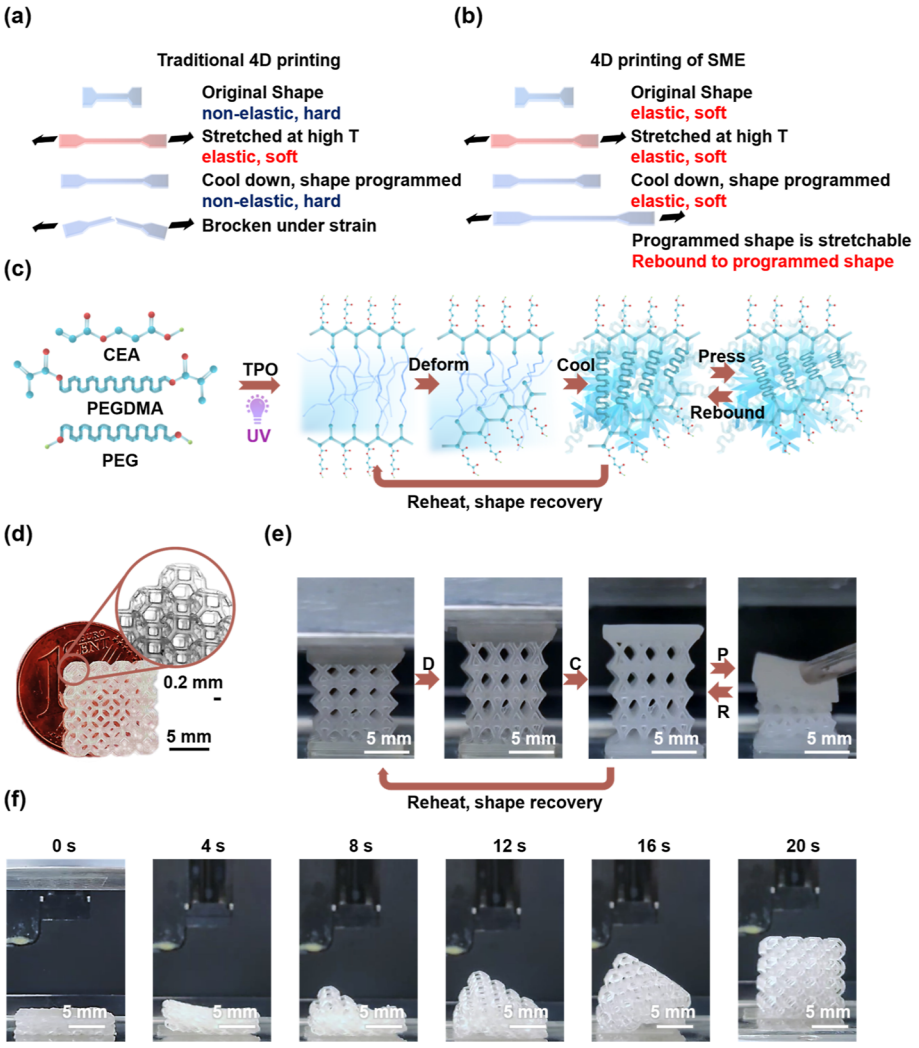


Figure 1. Principle, material system, and example of flexible 4D printed shape-memory elastomers: (a) the traditional 4D printed shape-memory polymer (SMP) can achieve high stretchability in its programmable state, but its fixed state is not elastic. (b) The 4D printed shape-memory elastomer (SME) is elastic not only in its programmable state but also in its fixed state, and the fixed state has fatigue resistance and can always recover to its programmed shape. (c) Material system and shape-memory mechanism for printing a PEG-based shape-memory elastomer: acrylate-based monomer CEA and PEGDMA are mixed with PEG and polymerized into the polymeric network. The PEG segments in the polymer network can crystallize and increase the stiffness of the material, while the crystalline state is still elastic and soft. (d) Printed shape-memory elastomer lattice, with a feature size of 150 μm. (e) Example of the printed shape-memory elastomer: the printed lattice part can be programmed in high temperature and fixed in low temperature, yet the fixed state is elastic. D = Deform, C = Cool, P = Press, R = Rebound. (f) Shape recovery process of a compressed 3D printed shape-memory elastomer lattice: the shape recovery process can be completed in 20 s.

are the localized photopolymerization of specific patterns of each layer using either a laser or a digital mirror device (DMD) that easily allows to reach resolutions below 200 μm.[24] Using SLA- or DLP-based printing, a series of (four-dimensional) 4D printing materials have been demonstrated, including meth-acrylated polycaprolactone (PCL),[25] *tert*-butyl acrylate (tBA)/diethylene glycol diacrylate (DEGDMA),[26] and polyurethane/isobornyl acrylate/DEGDMA systems.[27] However, all afore-mentioned systems suffered from poor mechanical performance like inelasticity and hardness of the final prints, which limited their application scenarios.

Ge et al.[18] developed a novel aliphatic urethane diacrylate (AUD)/tBA-based system for 4D printing, resulting in printed parts which can achieve up to 1240% strain at the rubbery state below 80 °C. However, although AUD-tBA proved to be stretchable under lower temperature, after we repeated the same formulation, we found that the material exhibited significant creep rather than elastic deformations (Figure S1). Without blurring the concepts of plastic deformation and elastic deformation and taking this material as an example, conventional *SMPs* (Figure 1a) refer to the materials that do not show elastic behavior below the transition temperature which usually is the melting point T_m or the glass transition point T_g. Consequently, the potential applicability of these materials as elastic structural components, such as sealing, jointing, and cushioning parts, is constrained after undergoing programming.

In this paper, we extend the conventional shape-memory approach by the first demonstration of SMEs (Figure 1b) suitable for 4D printing. SMEs are tailored toward 4D printing as they have good elastic deformation even below the transition temperature, i.e., after being programmed. In other words, the material should show elastic deformation whether above or below the transition temperature, i.e., no creep phenomenon. SMPs with similar properties based on ionomers,[28] semi-

https://doi.org/10.1021/acsami.3c07436
ACS Appl. Mater. Interfaces 2023, 15, 40923−40932

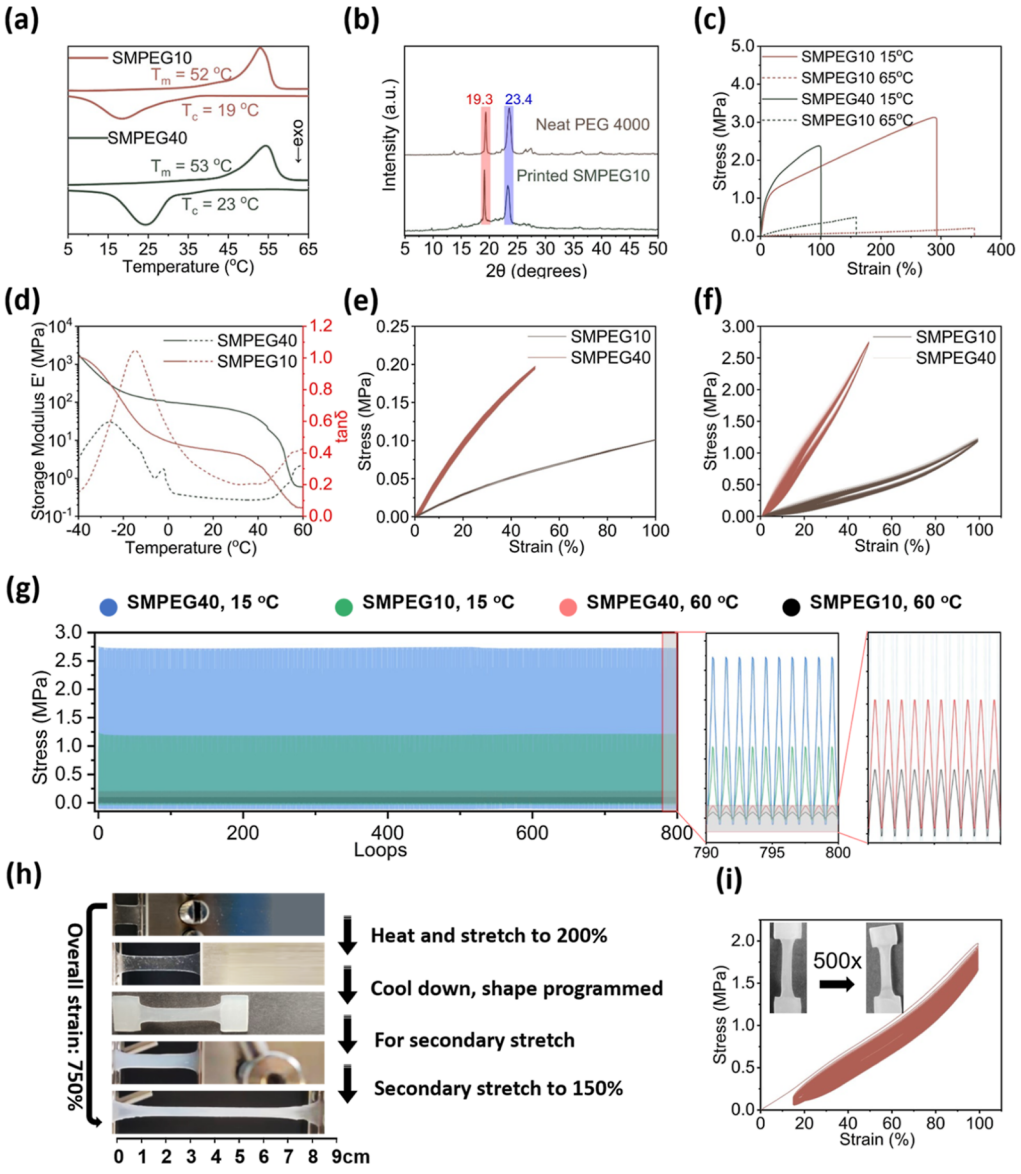


Figure 2. Characterization of the printed shape-memory elastomer: (a) DSC curves of SMPEG10 and SMPEG40 showing the melting points and the crystallization points. (b) XRD analysis result of printed SMPEG10 and neat PEG 4000, showing the PEG crystalline structure in SMPEG10. (c) Tensile test of SMPEG10 and SMPEG40 at 15 and 65 °C, indicating the stretchability of the materials under high and low temperatures. The materials possess a higher Young's Modulus at low temperatures compared to that at high temperatures. (d) DMA results of SMPEG10 and SMPEG40, the left axis and the solid line represent the storage modulus results, while the right axis and the dashed line represent the loss factor results. For both materials, their storage modulus exhibits a plateau between 0 and 40 °C and decreases after their melting point demonstrating the change on stiffness along with the temperature increment. Also, the low loss factor between 0 and 40 °C indicates the elasticity of the material in the temperature range. (e) Looping tensile test of SMPEG10 and SMPEG40 at 60 °C for 800 cycles. As can be seen, almost no creep occurs. (f) Looping tensile test of SMPEG10 and SMPEG40 at 15 °C for 800 cycles. At low temperatures, the material also shows a low creep due to no curve shifting shown along with cycling. (g) Relationship between generated stress and looping times of SMPEG10 and SMPEG40 according to (e,f); the result shows high elasticity and low creep of the materials at different temperatures. (h) Testing procedure of tensile test on a programmed SMPEG10 part with a fixed strain of 200%. The prestretched dogbone-shaped part can be further stretched to 150%. (i) Looping tensile test of the 200% prestretched SMPEG10 part for 500 cycles, the part is not broken, cracked, or shrank into the unprogrammed state after looping test.

crystals,[29] or liquid crystals[30,31] have been reported by the Mandelbaum and Mather. However, the focus of our work is the development of a formulation suitable for 3D printing. We present a successful implementation of 4D printing of SME utilizing a resin formulation based on polyethyleneglycol (PEG), a nontoxic and ecofriendly material with a high production yield and low cost. As a crystallizable polymer, PEG also has the potential to be used to make shape-memory materials.[32] However, if high elasticity is to be obtained (strain > 200%), PEG usually needs to be incorporated in the form of a hydrogel network,[33] which discourages its crystallization. By using 2-carboxylethylacrylate (CEA) as a dispersant for PEG instead of water, we developed a formulation which not only solubilizes PEG but also acts as the monomer which can be polymerized using free-radical polymerization, while the material could behave as a crystallization-controlled SME (Figure 1c). We applied a formulation including CEA, PEG, and a self-synthesized cross-linker PEG-dimethacrylate (PEGDMA, with a molecular weight of 10,000 g/mol) in DLP printing, showing that the material can be printed with high accuracy, i.e., with

https://doi.org/10.1021/acsami.3c07436
ACS Appl. Mater. Interfaces 2023, 15, 40923−40932

feature sizes smaller than 200 μm (Figure 1d). The elasticity of this SME is demonstrated in Figure 1e and Video S1, where the material can not only be manipulated and altered like a regular SMP but also showcase flexibility below the transition point. The material's thermal response is rapid, as depicted in Figure 1f and Video S2, as it regains its original shape within 20 s. This material facilitates DLP production of SMEs and is likely to be utilized in various engineering applications, such as programmable soft actuators and artificial muscles.

RESULTS AND DISCUSSION

Our DLP light-curing resin is composed of a cross-linker PEGDMA and a monomer blend of CEA (44.8 wt %), PEG 4000 (34.4 wt %), and PEG 400 (20.8 wt %). Here, we prepared two formulations, where SMPEG10 was prepared by mixing 10 wt % PEGDMA and 90 wt % monomer blend and SMPEG40 which was prepared by mixing 40 wt % PEGDMA and 60 wt % monomer blends. The resin is formulated to allow high-molecular-weight PEG to remain in the liquid state at the printing temperature thus preventing precipitation during the printing process, which is important for printing accurate structures. Following successful printing, the specimens underwent a drying process subsequent to being rinsed with isopropyl alcohol. To verify that the isopropyl alcohol does not rinse out the PEG from the specimens, we immersed the printed SMPEG10 specimens in a 60 °C isopropyl alcohol solution for 30 min. Subsequently, the specimens underwent ultrasonic development, followed by vacuum drying. Notably, the final mass of the specimens yielded 97.2 ± 0.34% of their initial mass, indicating that the isopropyl alcohol rinse does remove only a very small fraction from the material. Due to the different cross-linker ratios, we expected these mixtures to have different mechanical properties. Crystallization temperature (T_c) and melting temperature of the materials were measured using differential scanning calorimetry (DSC, Figure 2a). T_m and T_c were in a temperature range between 52−53 °C and 19−34 °C, respectively. Thus, we defined 60 °C as the "high temperature" where the PEG crystals were fully melted and 15 °C as "low temperature" where PEG chains were fully crystallized. We also observed the crystallization rate of SMPEG10 and SMPEG40 for nonisothermal conditions, i.e., different cooling rates. According to Figure S2, both SMPEG10 and SMPEG40 were able to complete crystallization within 2 min when the cooling rate reached 10 K/min. Also, the presence of PEG crystals was confirmed based on XRD results, and we performed XRD analysis of a SMPEG10 solid at 15 °C and compared the results with PEG4000, the results of which are shown in Figure 2b. As can be seen, peaks can be found at 19.3 and 23.4°, which correspond well with the peaks of pure PEG 4000.[34] Tensile tests were performed at 60 °C and 15 °C, and maximum elongation as well as Young's modulus of the printed materials was measured (Figure 2c). We found that SMPEG10 can be stretched to 364 and 302% at 60 and 15 °C with Young's moduli of 0.09 and 11.26 MPa, respectively. In comparison, SMPEG40 can only be stretched to 153 and 97% at these two temperatures but demonstrated higher Young's moduli of 26.16 and 0.58 MPa, respectively (Figure S3). The results demonstrate that, on the one hand, the presence of PEG crystals is indeed able to enhance the stiffness of the material; on the other hand, a higher concentration of cross-linker also leads to a higher modulus. That is to say, SMPEG40 exhibits a higher modulus at low temperature compared to SMPEG10, possibly due to its higher cross-linking and higher crystallinity. However, in the presence of PEG crystals, although the modulus of the material is increased, the material is stretchable at both high and low temperatures. Since in previous studies of SMPs, the shape of the material being programmed is always in its low-temperature state (below T_g or T_c), the properties of the material in this state determine the nature of the material when it is programmed. Next, we wanted to know if the stretching of SMPEGs at low and high temperatures is an elastic deformation. According to the results of DMA, the loss factor of both SMPEG10 and SMPEG40 is lower than 0.5 in the interval of 20−40 °C, which indicates that the materials possess elastic deformation ability (Figure 2d).

Creep and fatigue behavior were tested by repetitive stretching using cyclic tensile tests for SMPEG10 and SMPEG40 at 15 and 60 °C, respectively, with each set of tests comprising 800 tensile−recovery cycles. For SMPEG10, we chose 100% strain as the target value for each cycle, and for SMPEG40, we chose 50% due to its lower stretchability. Figure 2e shows the results of tensile cycling at high temperature. We find that both SMPEG10 and SMPEG40 show elastic deformation due to their rapid recovery, and no curve displacement due to creep. The curves of tensile and recovery overlap. And, in the results of the cyclic tensile test at low temperatures in Figure 2f, SMPEG10 and SMPEG40 were essentially creep-free. It is to be noted that the sample being stretched in this experiment was not prestretched. Figure 2g shows the results for all the above tests showing the elastic behavior of the above materials at low and high temperatures more clearly. As can be seen, the different elasticity tests cover a completely different range, where the cyclic stresses generated by the material at high temperatures (red and black) are much lower than its results at low temperatures (blue and green). Satisfactorily, the stresses generated by the material are essentially unchanged from the beginning to the end, indicating that the material is highly elastic regardless of the temperature. Across all 800 cycles, SMPEG10 and SMPEG40 show almost no hysteresis, which is a good indication of the fatigue resistance of the material at different temperatures.

In addition to the previous experiments, we performed tensile tests on SMPEG10 samples that were 200% prestretched. In this work, prestretching is the process of heating the sample, stretching it to 200%, cooling it, and thus programming the stretched state into the fixed deformation. This test is crucial as we need to determine if the prestretched sample will lose its stretchability or programmed shape. In Figure 2h, we illustrate the steps and result of this experiment, which proved that the SMPEG10 sample could stretch up to 150% even when it was prestretched by 200%. Figure 2i depicts the results of 500 cycles of tensile testing of the SMPEG10 sample prestretched by 200% at 15 °C and 100% strain. We observed that although prestretched SMPEG10 displayed some creep, it did not exhibit severe fatigue or damage due to prestretching. Furthermore, the programmed shape of the sample was maintained even after several stretches, demonstrating its robustness. This effectively demonstrates that SMEs can be programmed to still behave as stretchable elastomers. The experiment also demonstrates that the low-temperature elasticity in Video S1 is not solely due to its lattice deformation but rather to the material's inherent elastic deformation properties at low temperatures.

We characterized the ratio of fixation and recovery to further evaluate the shape-memory properties of the material. The ratio of fixation (r_f) serves as a parameter to describe the programmable properties of the material. A higher r_f value

https://doi.org/10.1021/acsami.3c07436
ACS Appl. Mater. Interfaces 2023, 15, 40923−40932

closer to 100% indicates that the material can be deformed in a programmable manner. On the other hand, the ratio of recovery (r_r) is utilized to evaluate the shape-memory performance of the material. A r_r value approaching 100% implies that the material can fully regain its initial shape. The experiment consisted of a preparation step and four cycling steps, as detailed in Figure 3a.

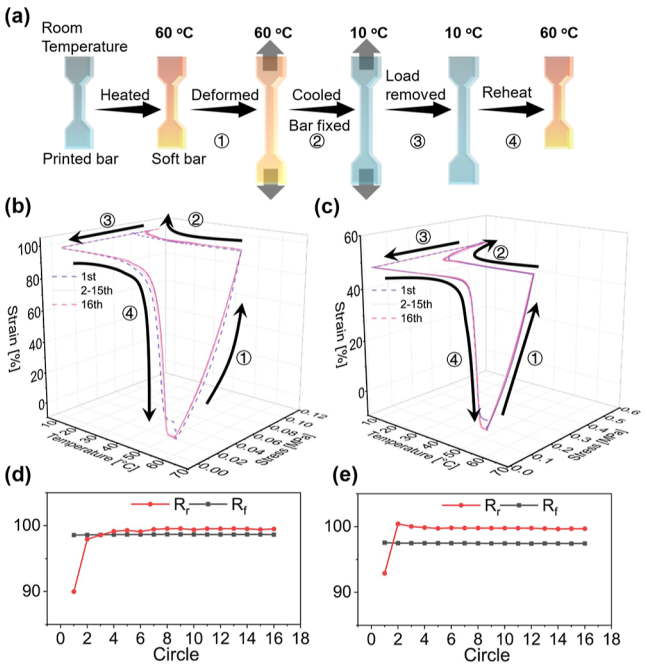


Figure 3. Characterization of shape-memory behavior of SMPEGs. (a) Test procedure of shape-memory tests. (b) 16-loops shape-memory cycle test with SPMEG10, the range of the temperature is 10−60 °C, the max strain is 100%, and the cycles do not show creep or weakening after 16 iterations. (c) 16-loops shape-memory cycle test with SPMEG40, the range of the temperature is 10−60 °C, the max strain is 50%, and the cycles do not show great creep or weakening. (d) Ratio of recovery r_r and ratio of fixation r_f of SMPEG10 from the 1st to the 16th cycles, from the 2nd cycle, the SMPEG has r_r and r_f over 97%. (e) The r_r and r_f of SMPEG40 from the 1st to the 16th cycles, from the 2nd cycle the SMPEG has r_r and r_f over 95%.

In the preparation step, the printed dogbone-shaped bar was placed on the test apparatus and heated to 60 °C. In the first cycling step, the bar was stretched under 60 °C to a specific strain. In the second step, the bar was maintained at this strain with a minimum stress, while it was cooled to 10 °C. In the third step, the fixation was gradually removed until the stress became zero. Finally, the bar was reheated to 60 °C without any load until it ceased to contract. This process was repeated for a total of 16 cycles. During the entire test, the strain, stress, and temperature were recorded using a DMA device at each stage, allowing us to generate 3D curve figures of the cycling test for analysis. The results of these experiments were used to evaluate the repeatability of the SMPEGs' shape-memory performance. Figure 3b,c shows the results of shape test cycles for SMPEG10 and SMPEG40, respectively. We calculated the results of r_f and r_r for each cycle separately. We found that r_f for SMPEG10 and SMPEG40 stays above 98% from the second cycle onward, demonstrating that they exhibit shape recovery of more than 97%. As can be seen, both SMPEGs do not only exhibit outstanding shape programmability but also excellent shape recoverability.

We demonstrated that the printed SMEs can also be microstructured using hot embossing. Such microstructuring can be used, e.g., to induce surface topographies as required for adjustable surface roughness or microfluidics. As illustrated in Figure 4a, we printed a dogbone with SMPEG10, heated it to 60 °C, and pressed it into a mold and fixed with two glass slides and clamped with a 33 mm office clip. The pressing was kept for 1 h in a 10 °C refrigerator to cool down the dogbone absolutely. Subsequently, we demolded the material and subjected it to cyclic stretching at 150% strain using a tensile tester. Figure 4b illustrates the surface structure of a 3D printed mold with a reverse text shape indentation with a depth and width of 200 μm. The programmed SMPEG10 part with the text embossed on the surface is shown in Figure 4c. Using an optical microscope, we can see that the text "neptunlab" is engraved on the surface of the component. After 400 stretching cycles, we can see that the structure of the text has not disappeared despite some slight distortion, which demonstrates the structural form-holding ability of the programmed material.

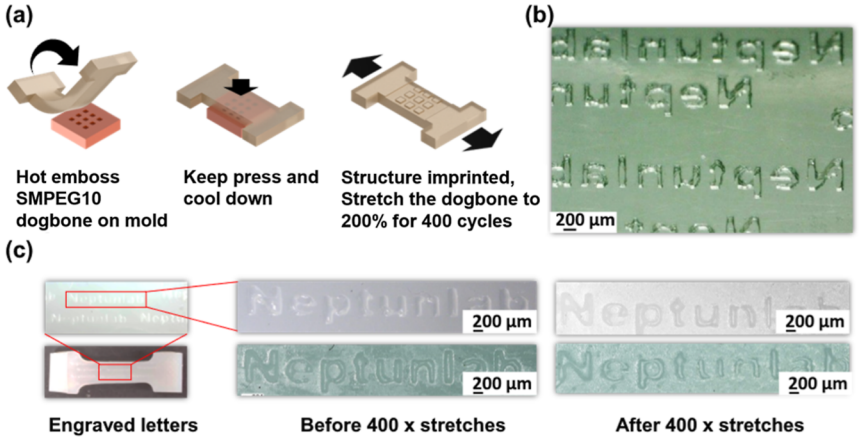


Figure 4. Microstructuring of printed SMPEGs. (a) Procedure to imprint specific structure on the surface of a SME dogbone: first, the printed dogbone was heated beyond its melting temperature and pressed onto a DLP printed perfluoropolyether[38] mold with negative surface texture. Afterward, while maintaining the pressure, the dogbone was cooled to 10 °C. After the mold was removed, the surface structure was imprinted and then the dogbone was stretched for 400 times to see if the surface structure was still present. (b) Structure of the molding using in (a). The width and depth of the letters is 200 μm. (c) Imprinted surface before and after 400 tensile cycles with 150% strain, indicating that the strain does not degrade the surface structures of the programmed shape thus demonstrating the robustness of shape programming.

https://doi.org/10.1021/acsami.3c07436
ACS Appl. Mater. Interfaces 2023, 15, 40923−40932

The high elasticity and stretchability of the developed material make them an interesting candidate for use as a programmable soft actuator or as a contractile storage material. As a first demonstrator, we have designed a pneumatic arm structure with adjacent hollow sphere structures with inward spherical concavities in the orthogonal direction of each sphere surface, as illustrated in Figure 5a. These concavities, referred to as

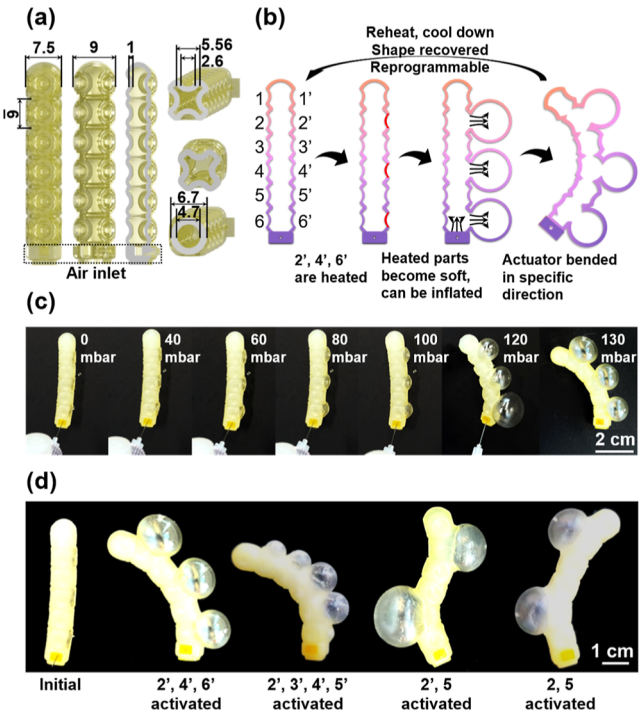


Figure 5. Structure, mechanism, and actuation result of programmable pneumatic actuators printed with SMPEG10. (a) Structure of the programmable pneumatic actuators, with the length of feature structures, the unit of each length is 1 mm. (b) Mechanism of programming and actuation of these actuators: First, the specific parts of the actuator were heated and become soft. Then, these parts could be inflated and expanded, the specific asymmetric expansion induce the programmed deformation (bending). (c) Actuation of one "2′,4′,6′-programmed" actuator over inner pressure. (d) Demonstration of the multiple feasibility of this programmable actuation system, the actuator was programmed in different ways and can realize different motivations with only one part, each example was actuated with 130 mbar inner pressure.

"thermally editable sites", will become low-modulus portions that are more likely to be expanded when pneumatically pressurized, resulting in an asymmetric expansion in Figure 5b. The membrane expansion is further amplified due to the nonlinear phenomenon of pressure−volume instability in balloons.[35] By heating the material above 60 °C, the programming of the actuator can be completely reset due to the use of the SME. Two-dimensional finite element analysis (2D-FEA) was initially used to simulate the behavior of the system (Figures S5 and S6), which showed the potential for fabricating the structure and achieving the desired results. The actuator was printed using SMPEG10, and an airtight inflation system was constructed using a multimaterial printing scheme according to our previous work.[36] After testing the actuator by heating specific thermally editable sites and pressurizing the actuators, successful bending in the predicted mode was observed at 140 mbar (Figure 5c), demonstrating the feasibility of a programmable pneumatic actuator (Video S3). The actuator can be programmed to move in various directions, including S-shaped flexure (Figure 5d). Finally, the programmed actuator can be reset by heating the whole actuator body (Video S4). Further technological advancements in this class of actuator are expected to include more complex structures and diverse thermal editing methods.

We further demonstrated that 4D printed SME can be used as a contractile storage material which could be of interest for applications like artificial muscles.[37] Therefore, a printed dogbone structure with SMPEG40 was heated and stretched to 100% strain, fixed, and cooled down (Figure 6a)). Subsequently, a 100 g weight was attached to the dogbone. The dogbone then shape-recovered by heating to 80 °C while lifting the weight (Figure 6b, Video S5). The recovery ratio versus time is shown in Figure 6c, illustrating that this size material is capable of pulling a 100 g weight while achieving an 80% shape recovery rate despite its self-weight of the stretched part is only 0.484 g.

CONCLUSIONS

In this study, we developed the first 4D printed SME utilizing PEG as the primary material. The elastomer is capable of stretching and elastically deforming at both high and low temperatures, serving as the programmable and programmed shape, respectively. We conducted cyclic tensile tests, which demonstrated the material's fatigue resistance to deformation at various temperatures. Furthermore, the material exhibited excellent shape-memory characteristics, as evidenced by its fixation and recovery ratio. The material's exceptional programmability and shape-memory properties offer a wide range of potential applications, including temperature-responsive surfaces, programmable flexible actuators, and artificial muscles. The programmable flexible actuators concept can bring forth innovative solutions for future soft robot development.

EXPERIMENTAL SECTION

Materials. Polyethylene glycol 10k (PEG10k), methacrylic anhydride (MAA), 4-dimethylaminopyridine (DMAP), polyethylene glycol 4000 (PEG4000), *tert*-butylacrylate (*t*BA), polyethylene glycol 400 (PEG400), 2-carboxyethyl acrylate (CEA), polyethylene glycol diacrylate 250 (PEGDA), diurethane dimethacrylate (DUDMA), pentaerythritol tetraacrylate (PETA), diphenyl-(2,4,6-trimethylbenzoyl)-phosphinoxide (TPO), acrylic acid (AA), and Sudan orange G (SOG) were purchased from Sigma-Aldrich. Aliphatic urethane diacrylate (AUD) or EBECRYL 8413 was obtained from Allnex. Phenol and 2-(5-chloro-2*H*-benzotriazole-2-yl)-6-(1,1-dimethyl ethyl)-4-methyl (Tinuvin 326) were supplied by BASF. Tetrahydrofuran (THF) and diethyl ether were sourced from Carl Roth.

All reagents were used as they were given without any pre-treatment. The cross-linker PEGDMA10k was synthesized according to a previous work of our group.[36]

Preparation of the Resins. All chemicals were weighted into a 250 mL brown bottle according to the formulations. For the shape-memory elastomers SMPEG10 and SMPEG40, the formulations are listed in Table 1. For the soft and hard materials applied in multimaterial printing programmable actuators, the formulations are displayed in Tables S2 and S3. The resin mixture was sonicated at 60 °C in an Elasonic 30H ultrasonic bath (Elma, Germany) for 30 min to yield a clear, homogenized resin. The yielded resins were directly applied for printing.

Digital Light Processing. The STL files were analyzed and sliced by the printing software Asiga Composer (Asiga, Erfurt, Germany). The dimension of the model is adjustable in the software. When printing balloons and actuators, setting the support at a height of 2 mm is

https://doi.org/10.1021/acsami.3c07436
ACS Appl. Mater. Interfaces 2023, 15, 40923−40932

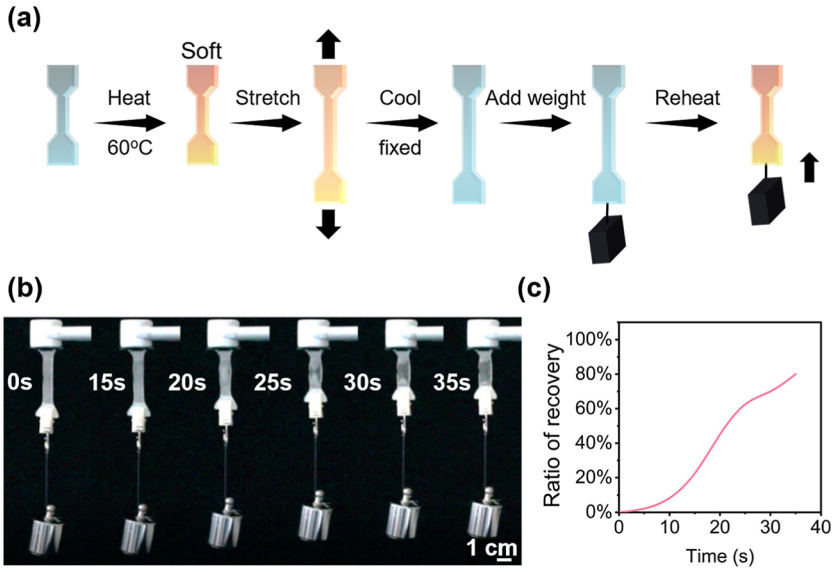


Figure 6. Demonstration of the weight lifting ability of the shape-memory elastomer SMPEG40. (a) Procedure to prepare a thermal responsive dogbone SME. (b) Demonstration of one SMPEG40 dogbone lifting a 100 g weight under heat (dogbone size: 20 mm × 10 mm × 2 mm, the mass of the actuated part is 0.484 g). (c) Relationship between recovery ratio and the heating time, indicating that the dogbone can recover 80% of the whole deformation after lifting 100 g weight.

Table 1. Formulation of SMPEG10 and SMPEG40

chemicals	SMPEG10 (wt %)	SMPEG40 (wt %)
PEG10kDMA	10	40
2-carboxyethyl acrylate	40	26.5
PEG4000	30.7	20.4
PEG400	18.4	12.2
DBTDL	0.5	0.5
Tinuvin 326	0.2	0.2
TPO	0.2	0.2

required. Printer Asiga Pico 2 (Asiga, Erfurt, Germany) was used for all the printings in this work, with a horizontal pixel resolution of 50 μm and a vertical resolution of 10 μm. The parameters of the device and the settings for the printing are listed in Table 2.

Table 2. Printing Settings

parameter	settings
layer thickness	0.05 mm
exposure dose	8.87 mW/cm^2
exposure time	2.7 s (SMPEG10, 40, 40C)
	3.8 s (Soft material)
	4.3 s (Hard material)
burn-in time	30 s
separation distance	6 mm (dogbone)
	16 mm (balloon/actuator)
printing temperature	50 °C
Z-compensation	0.05 mm
XY-compensation	0
support height (if need)	2 mm

The printing of a simple dogbone-shaped structure was performed with the parameters listed in Table 2. Compared with that, the programmable actuator structure is a multimaterial structure with air-tightening valve and printed in the order displayed in Table S4. In multimaterial 3D printing, the settings for each material remained unchanged. After one material was printed, it underwent a 20 s soaking process in 2-propanol to remove residual resin. The part was then dried using nitrogen before printing the next material. To remove the resin from inner volumes of the actuator, the solvent was slightly stirred. Since the base platform was not relocated after the first material was printed, there was no need to address any alignment issues. Once the resin tank was changed, the second material was printed with the same printing parameters.

After printing, the components underwent cleaning processes, starting with flushing with ethanol. The internal surfaces of actuators were cleaned by injecting solvent into them using a syringe. Following this, the parts were post-cured using a UV Curing chamber (XYZprinting, Neuss, Germany) for 20 min (intensity of 0.2 W/cm^2).

Hot Embossing. We used a previously reported 3D printed perfluoropolyether material[38] to print a mold containing mirror text texture, where the depth and the size of the text were 200 μm. A SMPEG10 specimen was fabricated by DLP, with a size of 35 mm × 10 mm × 2 mm. The specimen was first heated to 60 °C, with one side covered with a glass slide and the other side was pressed into the mold and fixed with a clamp. The sample was then cooled to 10 °C for 1 h to complete shape programming. At last, the specimen was removed from the mold to obtain surface structure.

Material Characterization. XRD measurements were obtained by a diffractometer D8 Discover (BRUKER AXS, USA) at room temperature with a LynxEye XE-T-Detector and Cu/K radiation (0.154060 nm). The patterns were recorded in the range of $2\theta = 5-50°$ with steps of 0.05°.

The calculation of crystallinity is according to the following equation in which X_C refers to crystallinity degree and A_c and A_a refer to the integral area of the XRD spectroscopy of the crystalline part and amorphous part, respectively[39]

$$X_c = \frac{A_c}{A_c + A_a} \times 100\% \quad (1)$$

The melting temperature (T_m) and crystallization temperature (T_c) of the SME were measured by F1 Phoenix (NETZSCH, Waldkraiburg, Germany). Samples (40 mg) were heated to 100 °C at a rate of 5 °C/min. Subsequently, the samples were cooled down to 10 °C, and the measurements proceeded from 10 °C to 100 °C at a heating and cooling rate of 5 °C/min. For the nonisothermal DSC experiments for calculating the kinetics of the crystallization, the samples were heated to 100 °C at a rate of 30 °C/min and then cooled down to 10 °C at rates of 10, 8, 6, and 4 °C/min. The calculation of $X(T)$, namely the relative crystallinity at temperature T, is carried out by the following equation, where the dH_c/dT refers the heat flow of crystalline at T[40,41]

https://doi.org/10.1021/acsami.3c07436
ACS Appl. Mater. Interfaces 2023, 15, 40923−40932

$$X(T) = \frac{\int_{T_0}^{T} \frac{dH_c}{dT} dT}{\int_{T_0}^{\infty} \frac{dH_c}{dT} dT} \times 100\% \quad (2)$$

The tensile test was performed by a tensile tester (Hegewald & Peschke Universal Testing Machine, Nossen, Germany) with a load cell of 100 N. A preload of 0.05 N was set, and the stretching rate was 40 mm/min. The dimension of the dogbone-formed sample was 10 mm × 10 mm × 1 mm.

The DMA test was performed by a Rheometer MCR 702 (Anton Paar, Ostfildern-Scharnhausen, Germany). The temperature range was from −40 to 65 °C, the heating rate was 3 °C/min, and the frequency was 2 Hz. The dimension of the sample was 10 mm × 5 mm × 1 mm.

The cyclic tensile test to characterize fatigue resistance was performed using a Rheometer MCR 702 (Anton Paar, Ostfildern-Scharnhausen, Germany). The dimension of the sample was 10 mm × 5 mm × 1 mm. SMPEG10 was stretched to 100% and returned to 0% at a speed of 16%/s at 25 and 60 °C, respectively. SMPEG40 was stretched to 50% and returned to 0% at a stretching speed of 12.5%/s at 25 and 60 °C, respectively. The process was repeated 800 times.

The shape-memory cyclic test was performed using a Rheometer MCR 702 (Anton Paar, Ostfildern-Scharnhausen, Germany). The cyclic test went through 4 steps, including stretching in the soft state, cooling down to fix the deformation, stress being removed, and reheating to recover the original shape. The dimension of the sample was 5 mm × 5 mm × 1 mm. The procedure of each step was completed according to Table S5. The ratio of fixation r_f and ratio of recovery r_r are calculated according to the following equations

$$r_f = \frac{\varepsilon_{unload}}{\varepsilon_{load}} \cdot 100\% \quad (3)$$

$$r_r = \frac{\varepsilon_{initial} - \varepsilon_{final}}{\varepsilon_{initial}} \cdot 100\% \quad (4)$$

The actuator was heated using a heated glass rod with a diameter of 3 mm, which was preheated in the oven at 80 °C. The inflation of the actuator was carried out by the accurate pump FLOW-EZ (FLUIGENT, Le Kremlin-Bicêtre, France). The needle was stuck into the inflation port to inflate the balloon with 140 mbar to observe the programmable actuation. Also, to keep the internal pressure, the needle can be removed directly without any additional air-tightening procedures due to the existence of a multimaterial air-tightening valve.

■ ASSOCIATED CONTENT

Supporting Information

The Supporting Information is available free of charge at https://pubs.acs.org/doi/10.1021/acsami.3c07436.

Elasticity of the SME (MP4)

Material regaining its original shape within 20 s (MP4)

Testing of the actuator by heating specific thermally editable sites and pressurizing the actuators, with successful bending in the predicted mode (MP4)

Programmed actuator reset by heating the whole actuator body (MP4)

Dogbone shape recovered by heating to 80 °C while lifting the weight (MP4)

Result of the strain-recovery experiment of the AUD-*t*BA material (with 5 wt % AUD) in room temperature; statistics of the tensile tests of SMPEG10 and SMPEG40, with error bars based on five parallel sets of tensile tests; two-dimensional finite element analysis (2D-FEA) to analogue programmable soft actuators; more detailed analysis of a single balloon expansion in a two-segmented robot; formulation of the resin for printing a soft material; formulation of the resin for printing a hard material; printing ranges of the multimaterial actuator; and procedure settled in a cycling shape memory test (PDF)

■ AUTHOR INFORMATION

Corresponding Author

Frederik Kotz-Helmer − *Laboratory of Process Technology, Department of Microsystems Engineering (IMTEK), NeptunLab, Freiburg 79110, Germany; Freiburg Materials Research Center (FMF), University of Freiburg, Freiburg 79085, Germany;* orcid.org/0000-0001-8376-154X; Email: frederik.kotz-helmer@neptunlab.org

Authors

Qingchuan Song − *Laboratory of Process Technology, Department of Microsystems Engineering (IMTEK), NeptunLab, Freiburg 79110, Germany; Cluster of Excellence livMatS @ FIT − Freiburg Center for Interactive Materials and Bioinspired Technologies, University of Freiburg, D-79110 Freiburg, Germany*

Yunong Chen − *Laboratory of Process Technology, Department of Microsystems Engineering (IMTEK), NeptunLab, Freiburg 79110, Germany*

Viacheslav Slesarenko − *Cluster of Excellence livMatS @ FIT − Freiburg Center for Interactive Materials and Bioinspired Technologies, University of Freiburg, D-79110 Freiburg, Germany*

Pang Zhu − *Laboratory of Process Technology, Department of Microsystems Engineering (IMTEK), NeptunLab, Freiburg 79110, Germany*

Ahmed Hamza − *Laboratory of Process Technology, Department of Microsystems Engineering (IMTEK), NeptunLab, Freiburg 79110, Germany*

Peilong Hou − *Laboratory of Process Technology, Department of Microsystems Engineering (IMTEK), NeptunLab, Freiburg 79110, Germany;* orcid.org/0000-0002-2572-9282

Dorothea Helmer − *Laboratory of Process Technology, Department of Microsystems Engineering (IMTEK), NeptunLab, Freiburg 79110, Germany; Cluster of Excellence livMatS @ FIT − Freiburg Center for Interactive Materials and Bioinspired Technologies, University of Freiburg, D-79110 Freiburg, Germany; Freiburg Materials Research Center (FMF), University of Freiburg, Freiburg 79085, Germany*

Bastian E. Rapp − *Laboratory of Process Technology, Department of Microsystems Engineering (IMTEK), NeptunLab, Freiburg 79110, Germany; Cluster of Excellence livMatS @ FIT − Freiburg Center for Interactive Materials and Bioinspired Technologies, University of Freiburg, D-79110 Freiburg, Germany; Freiburg Materials Research Center (FMF), University of Freiburg, Freiburg 79085, Germany;* orcid.org/0000-0002-3955-0291

Complete contact information is available at: https://pubs.acs.org/10.1021/acsami.3c07436

Author Contributions

F.K. and B.E.R supervised the whole project. Q.S., Y.C., and A.H. conceived the experiments. V.S. contributed to the simulation of programmable actuators. P.Z. and P.C. advised the resin formulation. Q.S. wrote the manuscript draft. F.K., B.E.R., and D.H. proofread the manuscript. All authors commented on the paper.

Notes

The authors declare no competing financial interest.

https://doi.org/10.1021/acsami.3c07436
ACS Appl. Mater. Interfaces 2023, 15, 40923−40932

■ ACKNOWLEDGMENTS

Funded by the Deutsche Forschungsgemeinschaft (DFG, German Research Foundation) under Germany's Excellence Strategy—EXC-2193/1-390951807. Also, this project has received funding from the European Research Council (ERC) under the European Union's Horizon 2020 research and innovation program (grant agreement no. 816006). Moreover, this work is part of the Research Cluster "Interactive and Programmable Materials (IPROM)" funded by the Carl Zeiss Foundation.

■ REFERENCES

(1) Huang, X.; Ford, M.; Patterson, Z. J.; Zarepoor, M.; Pan, C.; Majidi, C. Shape Memory Materials for Electrically-Powered Soft Machines. *J. Mater. Chem. B* **2020**, *8*, 4539−4551.
(2) Jin, B.; Song, H.; Jiang, R.; Song, J.; Zhao, Q.; Xie, T. Programming a Crystalline Shape Memory Polymer Network with Thermo- and Photo-Reversible Bonds toward a Single-Component Soft Robot. *Sci. Adv.* **2018**, *4*, No. eaao3865.
(3) Kim, Y.; Lim, Y.; Cha, D. E.; Kim, D. Simulation of Reversible Plasticity Shape Memory Polymer with Designed Strain Rate Dependent Failure Model. *Multiscale Sci. Eng.* **2021**, *3*, 88−94.
(4) Xiao, R.; Huang, W. M. Heating/Solvent Responsive Shape-Memory Polymers for Implant Biomedical Devices in Minimally Invasive Surgery: Current Status and Challenge. *Macromol. Biosci.* **2020**, *20*, 2000108.
(5) Song, C. History and Current Situation of Shape Memory Alloys Devices for Minimally Invasive Surgery. *Open Med. Devices J.* **2010**, *2*, 24−31.
(6) Maroni, A.; Melocchi, A.; Zema, L.; Foppoli, A.; Gazzaniga, A. Retentive Drug Delivery Systems Based on Shape Memory Materials. *J. Appl. Polym. Sci.* **2020**, *137*, 48798.
(7) Xu, H.; Yu, C.; Wang, S.; Malyarchuk, V.; Xie, T.; Rogers, J. A. Deformable, Programmable, and Shape-Memorizing Micro-Optics. *Adv. Funct. Mater.* **2013**, *23*, 3299−3306.
(8) Pretsch, T.; Ecker, M.; Schildhauer, M.; Maskos, M. Switchable Information Carriers Based on Shape Memory Polymer. *J. Mater. Chem.* **2012**, *22*, 7757−7766.
(9) Zhao, X.; Dong, R.; Guo, B.; Ma, P. X. Dopamine-Incorporated Dual Bioactive Electroactive Shape Memory Polyurethane Elastomers with Physiological Shape Recovery Temperature, High Stretchability, and Enhanced C2C12 Myogenic Differentiation. *ACS Appl. Mater. Interfaces* **2017**, *9*, 29595−29611.
(10) Chu, H.; Yang, W.; Sun, L.; Cai, S.; Yang, R.; Liang, W.; Yu, H.; Liu, L. 4D Printing: A Review on Recent Progresses. *Micromachines* **2020**, *11*, 796.
(11) Bakarich, S. E.; Gorkin, R.; Panhuis, M.; Spinks, G. M.; Spinks, G. M. 4D Printing with Mechanically Robust, Thermally Actuating Hydrogels. *Macromol. Rapid Commun.* **2015**, *36*, 1211−1217.
(12) Bodaghi, M.; Serjouei, A.; Zolfagharian, A.; Fotouhi, M.; Rahman, H.; Durand, D. Reversible Energy Absorbing Meta-Sandwiches by FDM 4D Printing. *Int. J. Mech. Sci.* **2020**, *173*, 105451.
(13) Cheng, C.-Y.; Xie, H.; Xu, Z.; Li, L.; Jiang, M.-N.; Tang, L.; Yang, K.-K.; Wang, Y.-Z. 4D Printing of Shape Memory Aliphatic Copolyester via UV-Assisted FDM Strategy for Medical Protective Devices. *Chem. Eng. J.* **2020**, *396*, 125242.
(14) Wu, J.-J.; Huang, L.-M.; Zhao, Q.; Xie, T. 4D Printing: History and Recent Progress. *Chin. J. Polym. Sci.* **2018**, *36*, 563−575.
(15) Kuang, X.; Roach, D. J.; Wu, J.; Hamel, C. M.; Ding, Z.; Wang, T.; Dunn, M. L.; Qi, H. J. Advances in 4D Printing: Materials and Applications. *Adv. Funct. Mater.* **2019**, *29*, 1805290.
(16) Nguyen, T. T.; Kim, J. 4D-Printing — Fused Deposition Modeling Printing and PolyJet Printing with Shape Memory Polymers Composite. *Fibers Polym.* **2020**, *21*, 2364−2372.
(17) Ge, Q.; Sakhaei, A. H.; Lee, H.; Dunn, C. K.; Fang, N. X.; Dunn, M. L. Multimaterial 4D Printing with Tailorable Shape Memory Polymers. *Sci. Rep.* **2016**, *6*, 31110.
(18) Zhang, B.; Li, H.; Cheng, J.; Ye, H.; Sakhaei, A. H.; Yuan, C.; Rao, P.; Zhang, Y.-F.; Chen, Z.; Wang, R.; He, X.; Liu, J.; Xiao, R.; Qu, S.; Ge, Q. Mechanically Robust and UV-Curable Shape-Memory Polymers for Digital Light Processing Based 4D Printing. *Adv. Mater.* **2021**, *33*, 2101298.
(19) Comb, J.; Priedeman, W.; Turley, P. W. *FDM® Technology Process Improvements*, 1994.
(20) Chacón, J. M.; Caminero, M. A.; García-Plaza, E.; Núñez, P. J. Additive Manufacturing of PLA Structures Using Fused Deposition Modelling: Effect of Process Parameters on Mechanical Properties and Their Optimal Selection. *Mater. Des.* **2017**, *124*, 143−157.
(21) Zhou, L.-Y.; Fu, J.; He, Y. A Review of 3D Printing Technologies for Soft Polymer Materials. *Adv. Funct. Mater.* **2020**, *30*, 2000187.
(22) Sydney Gladman, A.; Matsumoto, E. A.; Nuzzo, R. G.; Mahadevan, L.; Lewis, J. A. Biomimetic 4D Printing. *Nat. Mater.* **2016**, *15*, 413−418.
(23) Ong, L. J. Y.; Islam, A.; DasGupta, R.; Iyer, N. G.; Leo, H. L.; Toh, Y.-C. A 3D Printed Microfluidic Perfusion Device for Multicellular Spheroid Cultures. *Biofabrication* **2017**, *9*, 045005.
(24) Huang, J.; Qin, Q.; Wang, J. A Review of Stereolithography: Processes and Systems. *Processes* **2020**, *8*, 1138.
(25) Zarek, M.; Layani, M.; Eliazar, S.; Mansour, N.; Cooperstein, I.; Shukrun, E.; Szlar, A.; Cohn, D.; Magdassi, S. 4D Printing Shape Memory Polymers for Dynamic Jewellery and Fashionwear. *Virtual Phys. Prototyping* **2016**, *11*, 263−270.
(26) Choong, Y. Y. C.; Maleksaeedi, S.; Eng, H.; Su, P.-C.; Wei, J. Curing Characteristics of Shape Memory Polymers in 3D Projection and Laser Stereolithography. *Virtual Phys. Prototyping* **2017**, *12*, 77−84.
(27) Zhao, T.; Yu, R.; Li, X.; Cheng, B.; Zhang, Y.; Yang, X.; Zhao, X.; Zhao, Y.; Huang, W. 4D Printing of Shape Memory Polyurethane via Stereolithography. *Eur. Polym. J.* **2018**, *101*, 120−126.
(28) Weiss, R. A.; Izzo, E.; Mandelbaum, S. New Design of Shape Memory Polymers: Mixtures of an Elastomeric Ionomer and Low Molar Mass Fatty Acids and Their Salts. *Macromolecules* **2008**, *41*, 2978−2980.
(29) Luo, X.; Mather, P. T. Preparation and Characterization of Shape Memory Elastomeric Composites. *Macromolecules* **2009**, *42*, 7251−7253.
(30) Burke, K. A.; Mather, P. T. Soft Shape Memory in Main-Chain Liquid Crystalline Elastomers. *J. Mater. Chem.* **2010**, *20*, 3449−3457.
(31) Chung, T.; Romo-Uribe, A.; Mather, P. T. Two-Way Reversible Shape Memory in a Semicrystalline Network. *Macromolecules* **2008**, *41*, 184−192.
(32) Boumezgane, O.; Messori, M. Poly(Ethylene Glycol)-Based Shape-Memory Polymers. *Int. J. Polym. Anal. Charact.* **2017**, *22*, 463−471.
(33) Feng, L.; Jia, S.-S.; Chen, Y.; Liu, Y. Highly Elastic Slide-Ring Hydrogel with Good Recovery as Stretchable Supercapacitor. *Chem.—Eur. J.* **2020**, *26*, 14080−14084.
(34) Liu, R.; Lai, Y.; He, B.; Li, Y.; Wang, G.; Chang, S.; Gu, Z. Supramolecular Nanoparticles Generated by the Self-Assembly of Polyrotaxanes for Antitumor Drug Delivery. *Int. J. Nanomed.* **2012**, *7*, 5249−5258.
(35) *Rubber and Rubber Balloons: Paradigms of Thermodynamics*; Müller, I., Strehlow, P., Eds.; *Lecture Notes in Physics*; Springer Berlin Heidelberg: Berlin, Heidelberg, 2004; Vol. *637*.
(36) Song, Q.; Chen, Y.; Hou, P.; Zhu, P.; Helmer, D.; Kotz-Helmer, F.; Rapp, B. E. Fabrication of Multi-Material Pneumatic Actuators and Microactuators Using Stereolithography. *Micromachines* **2023**, *14*, 244.
(37) Song, J. J.; Chang, H. H.; Naguib, H. E. Biocompatible Shape Memory Polymer Actuators with High Force Capabilities. *Eur. Polym. J.* **2015**, *67*, 186−198.
(38) Kotz, F.; Risch, P.; Helmer, D.; Rapp, B. E. Highly Fluorinated Methacrylates for Optical 3D Printing of Microfluidic Devices. *Micromachines* **2018**, *9*, 115.
(39) Jain, K.; Madhu, G.; Bhunia, H.; Bajpai, P. K.; Nando, G. B.; Reddy, M. S. Physico-Mechanical Characterization and Biodegradability Behavior of Polypropylene/Poly(L-Lactide) Polymer Blends. *J. Polym. Eng.* **2015**, *35*, 407−415.

https://doi.org/10.1021/acsami.3c07436
ACS Appl. Mater. Interfaces 2023, 15, 40923−40932

(40) Zhang, J.; Chen, S.; Jin, J.; Shi, X.; Wang, X.; Xu, Z. Non-Isothermal Melt Crystallization Kinetics for Ethylene−Acrylic Acid Copolymer in Diluents via Thermally Induced Phase Separation. *J. Therm. Anal. Calorim.* **2010**, *101*, 243−254.
(41) Jhu, Y.-S.; Yang, T.-C.; Hung, K.-C.; Xu, J.-W.; Wu, T.-L.; Wu, J.-H. Nonisothermal Crystallization Kinetics of Acetylated Bamboo Fiber-Reinforced Polypropylene Composites. *Polymers* **2019**, *11*, 1078.

https://doi.org/10.1021/acsami.3c07436
ACS Appl. Mater. Interfaces 2023, 15, 40923−40932